

10
2-13-9195(1)

SLAC-PUB--4811
DE91 007414

BASIC OPTICS OF THE SLC FINAL FOCUS SYSTEM*

KARL L. BROWN

*Stanford Linear Accelerator Center
Stanford University, Stanford, California 94309*

ABSTRACT

In this report we discuss some general optics principles and scaling laws that have been useful in guiding the design and operation of the Final Focus System for the Stanford Linear Collider. Included are expressions for the minimum β_x^* and β_y^* that can be expected for the present SLC design at the interaction point as a function of beam emittance.

*Presented at the Workshop on the Physics of Linear Colliders, Capri, Italy,
June 13-17, 1988 and at the International Workshop on the Next Generation of Linear
Colliders, Stanford, CA, November 28-December 9, 1988*

*Work supported by the Department of Energy, contract DE-AC03-76SF00515.

MASTER

DISTRIBUTION OF THIS DOCUMENT IS UNLIMITED

EB

1. Introduction

One of the unique features of a linear collider is the Final Focus System (FFS) whose function is to demagnify a linac beam, of finite momentum spread, and bring it to an achromatic focus of the smallest possible dimensions in preparation for high luminosity beam-beam collisions.

This report discusses some general principles applicable to the SLC round beam design and provides some simple scaling laws that influenced the choice of the initial design parameters.

For purposes of discussion, we show in Fig. 1 a block diagram of the SLC Final Focus System consisting of three main subsections: a Beam Matching Section, a Chromatic Correction Section (CCS), and a Final Transformer (FT). Our discussion addresses the choice of the design parameters for the CCS and of the FT.

The principal problem to be solved in the optical design of a Final Focus System is the minimization of the chromatic distortions introduced by the final lens system nearest to the interaction point (I.P.). If the beam exiting the linac were monoenergetic then the FFS design would be relatively easy. It would consist of a simple first-order optical system demagnifying the linac beam to the small size needed for collisions at the I.P. The ultimate limitation would then be from the residual higher-order geometric aberrations of the optical system and/or from emittance growth caused by synchrotron radiation energy losses in the lens system.

Unfortunately particle beams from linear accelerators are not monoenergetic, but have a finite momentum spread. So it usually becomes necessary to compensate for the chromaticity of the FFS lattice. There are several factors that influence the solution of this problem.

1. A reduction in the momentum spread or of the emittance of the linac beam reduces the magnitude of the problem.
2. The chromatic distortion of a FFS lattice is a function of the distance, l^* , of the first lens from the I.P. The closer the lens system is to the I.P. the

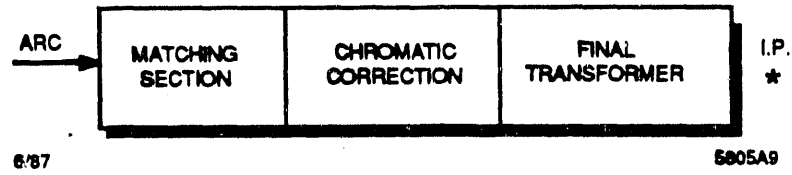


Fig. 1. A Block Diagram of the SLC Final Focus System.

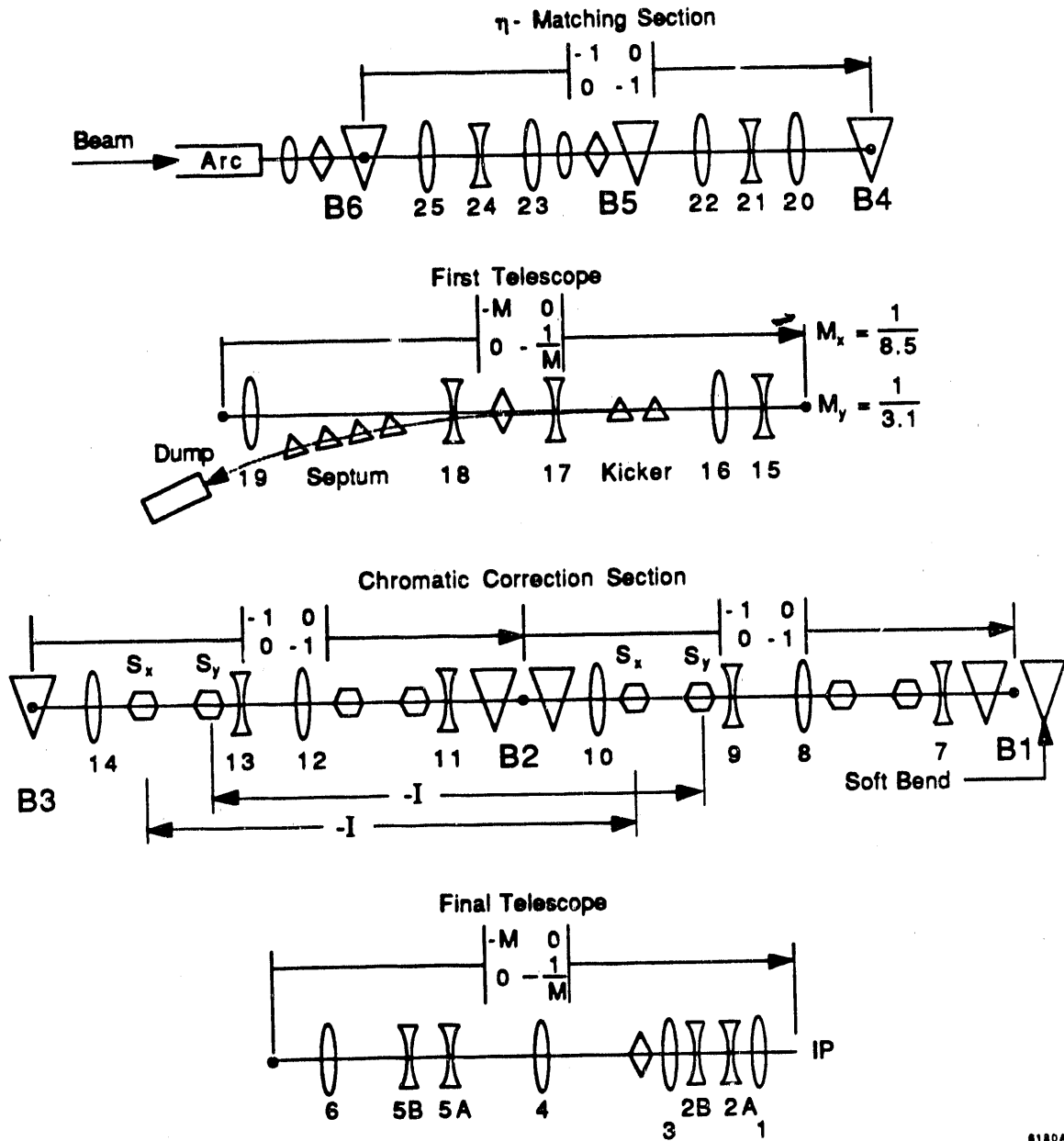
smaller the chromatic distortion. Hence strong, compact lenses near the I.P. are an asset to solving the problem. However the emittance growth caused by quantum fluctuations from the synchrotron radiation energy losses in the interaction region lens system will ultimately limit the smallest spot size that can be achieved.

3. Sextupoles in combination with dipoles (to provide dispersion) can be used to cancel the chromaticity of the lattice. Sextupoles introduced as pairs, with the elements of each pair separated by a minus unity optical transform, do not generate second-order geometric aberrations. Furthermore, if the chromatic correction section possesses repetitive symmetry and has a total transformation matrix of unity, then a potentially serious second-order chromatic aberration, $T_{166} = (x|\delta^2)$ is eliminated. However, there are other problems: The dipoles introduce emittance growth via synchrotron radiation. This complication imposes serious constraints on the location, strengths, and lengths of the dipoles so as to minimize this effect. In addition, the finite length of the sextupoles and optical cross-coupling between families of sextupoles generate higher-order geometric and chromatic aberrations which limit the ultimate beam spot size that can be achieved.

In summary, the basic problem in a final focus system design is to find a satisfactory balance among all of these competing factors so as to arrive at the maximum possible luminosity. The purpose of this paper is to derive some simple scaling laws, applicable to the SLC design, that provide a guide to the choice of the design parameters.

In Fig. 2 we show a detailed schematic diagram of the Stanford Linear Collider (SLC) Final Focus System as a representative example to illustrate the principal components and subsystems of a typical design. The triangular objects represent dipoles, the lens shaped objects are quadrupoles, and the hexagonal objects are sextupoles. The diamond shaped objects are skew quadrupoles used to minimize x - y cross-plane coupling at the interaction point.

In this design the CCS possesses repetitive symmetry and a total transforma-



12-88

6180A12

Fig. 2. A Detailed Schematic Diagram of the SLC Final Focus System.

tion matrix equal to the unity matrix. The sextupoles are inserted as pairs, with the elements of each pair separated by minus the unity matrix. The system is also designed to have a beam envelope waist, in both the x and y transverse planes, positioned at the center of dipole B3 in the CCS and at all positions that are a multiple of π phase shift downstream of this position, such as at the centers of B2 and B1. All of these factors are important in order to minimize the aberrations of the system.

2. Definitions and Notation

For the theoretical discussion, we use the six dimensional phase space parameters defined by the TRANSPORT^{1,2} notation; namely

$$\vec{X} = \begin{pmatrix} x_1 \\ x_2 \\ x_3 \\ x_4 \\ x_5 \\ x_6 \end{pmatrix} = \begin{pmatrix} x \\ x' \\ y \\ y' \\ l \\ \delta \end{pmatrix} \quad (1)$$

where $\delta = (p - p_0)/p_0$ and l is the path length difference.

The first, second, and third-order optics is represented by the R , T , and U matrix elements as follows:

$$x_i = \sum_{j=1}^6 R_{ij} x_j + \sum_{j,k=1}^6 T_{ijk} x_j x_k + \sum_{j,k,l=1}^6 U_{ijkl} x_j x_k x_l + \dots \quad (2)$$

For a system possessing midplane symmetry, the R matrix has the form:

$$R = \begin{pmatrix} R_{11} & R_{12} & 0 & 0 & 0 & R_{16} \\ R_{21} & R_{22} & 0 & 0 & 0 & R_{26} \\ 0 & 0 & R_{33} & R_{34} & 0 & 0 \\ 0 & 0 & R_{43} & R_{44} & 0 & 0 \\ R_{51} & R_{52} & 0 & 0 & 1 & R_{56} \\ 0 & 0 & 0 & 0 & 0 & 1 \end{pmatrix} \quad (3)$$

The initial objective in the SLC design was to find a way of eliminating all of the second-order geometric and chromatic aberrations, T_{ijk} , and be left with only the appropriate linear terms and the residual third- and higher-order aberrations. These residual aberrations combined with synchrotron radiation emittance growth and constraints imposed by the SLAC site then determined the minimum spot size that could be achieved at the interaction point.

3. Chromatic Aberrations

We use the Courant-Snyder notation β , γ and α to describe the transformation of a phase space ellipse from a position 0 to a position 1 in a beam transport line. β_1 at position 1 may be expressed as a function of the R matrix between position 0 and 1 and the values of the Courant-Snyder parameters β_0 , α_0 and γ_0 at position 0 via the equation²

$$\beta_1 = R_{11}^2 \beta_0 - 2 R_{11} R_{12} \alpha_0 + R_{12}^2 \gamma_0$$

where

$$\beta \gamma - \alpha^2 = 1$$

If we assume an upright ellipse, *i.e.* $\alpha_0 = 0$, at the beginning of the system, then the equation for β_1 simplifies to

$$\beta_1 = R_{11}^2 \beta_0 + \frac{R_{12}^2}{\beta_0} \quad (4)$$

We now define the matrix elements $R_{11}(\delta)$ and $R_{12}(\delta)$ for the x plane as,

$$R_{11}(\delta) = R_{11}(0) + \frac{\partial R_{11}}{\partial \delta} \delta + \frac{1}{2} \frac{\partial^2 R_{11}}{\partial \delta^2} \delta^2 + \dots = R_{11}(0) + T_{116} \delta + U_{1166} \delta^2 + \dots$$

$$R_{12}(\delta) = R_{12}(0) + \frac{\partial R_{12}}{\partial \delta} \delta + \frac{1}{2} \frac{\partial^2 R_{12}}{\partial \delta^2} \delta^2 + \dots = R_{12}(0) + T_{126} \delta + U_{1266} \delta^2 + \dots \quad (5)$$

where the partial derivatives are evaluated for $\delta = 0$. $R_{11}(0)$ and $R_{12}(0)$ are the values of the matrix elements for the central momentum p_0 . β_x^* at the I.P, as a function of momentum, is then expressed by the equation

$$\beta_x^*(\delta) = R_{11}^2(\delta) \beta_0 + \frac{R_{12}^2(\delta)}{\beta_0} \quad (6)$$

β_0 is the value of β_x at the beginning of the FFS, and R_{11} and R_{12} are matrix elements measured from the beginning of the FFS to the I.P. We assume that β_0 is independent of δ .

Ideally it is desired that β_x^* and β_y^* be independent of momentum. But, in practice, it is only possible to correct to some order in δ . For the SLC, where the sextupole families are interlaced, the system is corrected to second-order in the chromatic and geometric aberrations and the residual terms, limiting the performance of the system, begin with the third-order aberrations.

If, as in the SLC, the design is based on the use of telescopic modules^{2,3}, as illustrated in Figs. 3 and 4, then for the x plane we have:

$$R_{12}(0) = 0 \text{ because of point to point imaging.}$$

$$T_{116} \simeq 0 \text{ if the telescopic modules are symmetric as in Fig. 3.}$$

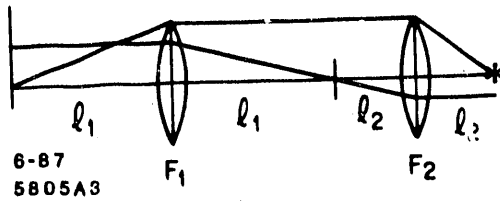


Fig. 3. A Thin Lens Telescopic Transformer.

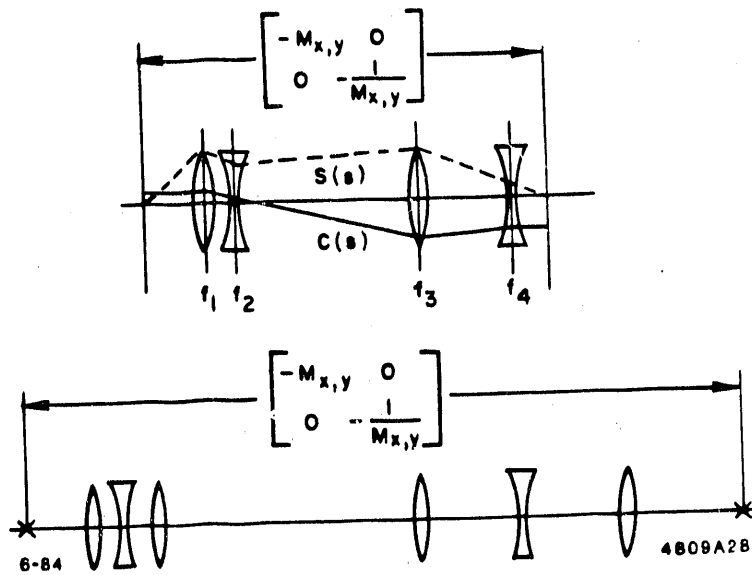


Fig. 4. Telescopic Transformers using Doublets and Triplets.

$R_{11}(0)$ = the demagnification in the x plane from the beginning of the FFS to the interaction point, and T_{126} can be made to vanish by the use of sextupoles.

Then, for the x plane, the dominant terms in the expansion become:

$$R_{11}(\delta) \simeq R_{11}(0) \quad \text{and} \quad R_{12}(\delta) \simeq U_{1266} \delta_x^2. \quad (7)$$

Substitution into Eq. (6) yields

$$\beta_x^*(\delta) \simeq \beta_x^*(0) + \frac{[R_{11}(0) U_{1266} \delta_x^2]^2}{\beta_x^*(0)}. \quad (8)$$

where $\beta_x^*(0) = R_{11}^2(0)\beta_0$ is the monoenergetic size of β_x at the I.P. and $[R_{11}(0) U_{1266}]$ is the magnitude of the dominant *residual chromatic distortion* in the x plane of the FFS. It should be noted here that if the entire length of the final focus system is scaled with l^* then the residual chromatic distortion, $[R_{11}(0) U_{1266}]$, also scales linearly with l^* . Similar results occur for the y plane optics.

We arbitrarily define the momentum bandwidth of the FFS as the value of $\delta_x = \delta_{25}$ for which $\beta(\delta)$ grows by 25 percent, *i.e.*

$$\beta(\delta_{25}) = 1.25 \beta^*(0). \quad (9)$$

Substituting into Eq. 8 we have for the x plane

$$\beta_x^*(0) \simeq 2R_{11}(0) U_{1266} \delta_x^2, \quad (10)$$

from which the momentum bandwidth in the x plane is

$$\delta_x \simeq \left[\frac{\beta_x^*(0)}{2 R_{11}(0) U_{1266}} \right]^{\frac{1}{2}}. \quad (11)$$

Similarly for the y plane the result is

$$\beta_y^*(0) \simeq 2R_{33}(0) U_{3466} \delta_y^2, \quad (12)$$

with a corresponding momentum bandwidth in the y plane of

$$\delta_y \simeq \left[\frac{\beta_y^*(0)}{2 R_{33}(0) U_{3466}} \right]^{\frac{1}{2}}. \quad (13)$$

Where U_{1266} and U_{3466} are *assumed* to be the dominant residual aberrations in

the x and y planes respectively. To assure that this is the case, we now discuss the geometric (monoenergetic) aberrations and a mechanism of controlling their magnitudes relative to the dominant chromatic terms.

4. Geometric Aberrations

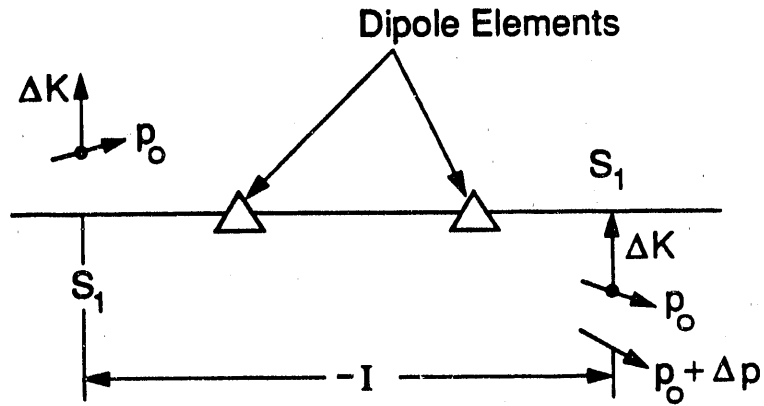
We define geometric aberrations as those which are associated with the monoenergetic trajectories in a beam transport system, *i.e.* for those trajectories having a momentum p_0 .

If the system is designed using sextupole pairs, separated by a minus unity optical transform as illustrated in Figs. 5 and 6, then all second-order geometric aberrations, introduced by the sextupoles, will vanish at the exit of the chromatic correction section, and the residual geometric aberrations will all be of third-order and higher. We note that separated function quadrupoles do not generate second-order geometric aberrations.

The magnitude of the residual geometric aberrations is a non-linear function of the betatron amplitudes that trajectories, having a momentum p_0 , experience as they traverse the optical system. Similarly, the magnitude of the chromatic aberrations is a non-linear function of the amplitudes of the *off momentum* trajectories as they traverse the system.

So it can be expected that the residual geometric and chromatic aberrations will be of comparable importance when the monoenergetic excursions of the beam and the chromatic excursions are approximately equal in magnitude.

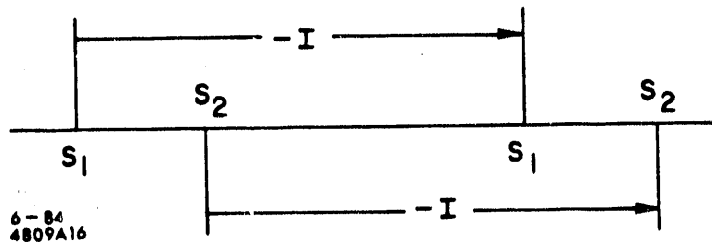
The controlling factor establishing this balance for the SLC design is the strength of the first dipole used in the Chromatic Correction Section (CCS). To quantify this concept we equate the monoenergetic angular spread of the beam exiting from the first CCS dipole to the chromatic angular spread created by the dipole. If we assume, as is the case in the SLC design, that there is a beam envelope waist in both the x and y planes at the center of the dipole, then this equality of the geometric and chromatic aberrations occurs when



11-88

6180A4

Fig. 5. A Minus Unity Transform between Sextupole Pairs



6-84
4809A16

Fig. 6. Interlaced Sextupole Families for Chromatic Corrections.

$$\sqrt{\frac{\epsilon_x}{\beta_{xD}}} \simeq \sqrt{\frac{\epsilon_y}{\beta_{yD}}} \simeq \alpha_D \cdot \delta_x \quad (14)$$

where α_D is the bending angle of the dipole, as illustrated in Fig. 7. ϵ_x and ϵ_y are the beam emittances in the x and y planes respectively, δ_x is the momentum bandwidth in the x plane and β_{xD} and β_{yD} are the values of the β functions at the center of the CCS dipole. Note that only δ_x and not δ_y appears in Eq. 14. This is because the SLC final focus system is designed with dispersion in the x plane only.

In the SLC final focus system, the most important residual x plane aberrations, as determined by TRANSPORT¹, are the third order terms: U_{1266} , U_{1446} , U_{1222} and U_{1244} . It is also found from TRANSPORT simulations that

$$U_{1266} = (x|x'\delta^2) \quad (15)$$

is independent of the magnitude of the bending angle α_D . Another, but less important chromatic aberration is

$$U_{1446} = (x|y'^2\delta), \quad (16)$$

whose magnitude varies approximately as $1/\alpha_D$.

The important residual geometric aberrations in the x plane are

$$U_{1222} = (x|x'^3) \quad \text{and} \quad U_{1244} = (x|x'y'^2). \quad (17)$$

whose magnitudes vary approximately as $1/\alpha_D^2$.

So we observe that the last three aberrations may be suppressed relative to the dominant chromatic aberration, U_{1266} , by just increasing the magnitude of the CCS dipole bending angle α_D . However, as will be discussed below, there is a practical limit to the maximum size of α_D that is allowed because of quantum fluctuations coming from synchrotron radiation energy losses in the dipoles.

Dipoles for the Chromatic Corrections

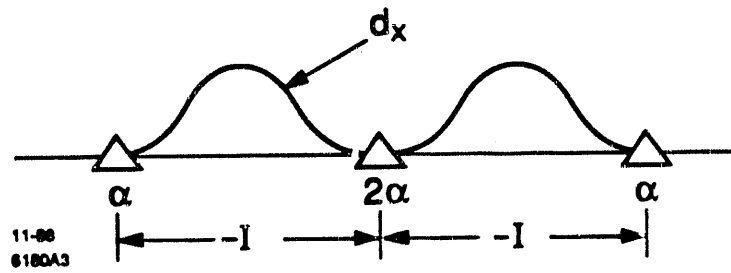


Fig. 7. Arrangement of Dipoles in the Chromatic Correction Section.

Similar residual chromatic and geometric aberrations occur in the y plane optics.

If we rewrite Eq. 14. in the form,

$$\delta_x^2 \simeq \frac{\epsilon_x}{\beta_{xD} \alpha_D^2} \simeq \frac{\epsilon_y}{\beta_{yD} \alpha_D^2} \quad (18)$$

and define the monoenergetic demagnifications M_x and M_y of the final telescopic transformer(FT) as

$$M_x = \sqrt{\frac{\beta_x^*(0)}{\beta_{xD}}} \quad M_y = \sqrt{\frac{\beta_y^*(0)}{\beta_{yD}}},$$

then it follows that

$$\delta_x^2 \simeq \frac{M_x^2 \epsilon_x}{\beta_x^*(0) \alpha_D^2} \simeq \frac{M_y^2 \epsilon_y}{\beta_y^*(0) \alpha_D^2} \quad (19)$$

Substituting Eq. 19 into Eq. 10, we conclude that the first-order monoenergetic beta function at the interaction point in the x plane is given by the expression

$$\beta_x^*(0) \simeq \frac{M_x}{\alpha_D} \cdot [2 \epsilon_x R_{11}(0) U_{1266}]^{\frac{1}{2}}, \quad (20)$$

and from Eq. 11, it follows that the momentum bandwidth in the x plane is

$$\delta_x \simeq \left[\frac{\beta_x^*(0)}{2 R_{11}(0) U_{1266}} \right]^{\frac{1}{2}} = \left[\frac{M_x^2 \epsilon_x}{2 \alpha_D^2 R_{11}(0) U_{1266}} \right]^{\frac{1}{4}}. \quad (21)$$

From Eq. 19 we conclude that the monoenergetic beta function in the y plane is

$$\beta_y^*(0) \simeq \left[\frac{M_y}{M_x} \right]^2 \cdot \left(\frac{\epsilon_y}{\epsilon_x} \right) \cdot \beta_x^*(0), \quad (22)$$

and from Eq. 13, we obtain the momentum bandwidth in the y plane

$$\delta_y \simeq \left[\frac{\beta_y^*(0)}{2 R_{33}(0) U_{3466}} \right]^{\frac{1}{2}}. \quad (23)$$

$\beta_x^*(0)$ and $\beta_y^*(0)$, as expressed by Eqs. 20 and 22, are the approximate values of the first-order monoenergetic beta functions at the interaction point when the

higher-order geometric and chromatic aberrations are approximately equal in magnitude. The corresponding first-order spot sizes $\sigma_x^*(0)$ and $\sigma_y^*(0)$ are then given by the equations

$$\sigma_x^*(0) = \sqrt{\beta_x^*(0) \cdot \epsilon_x} \quad \sigma_y^*(0) = \sqrt{\beta_y^*(0) \cdot \epsilon_y} \quad (XX)$$

If we set $M_x = M_y$, which it is for the present SLC design, then it follows from the above equations that

$$\frac{\sigma_y^*(0)}{\sigma_x^*(0)} = \frac{\beta_y^*(0)}{\beta_x^*(0)} = \frac{\epsilon_y}{\epsilon_x} \quad (YY)$$

One of the consequences of Eq.(YY) is that the first-order angular spread of the beam at the interaction point is the same in the x and y planes, independent of the ratio of the x and y emittances. *i.e.*

$$\theta_x^* = \sqrt{\frac{\epsilon_x}{\beta_x^*(0)}} = \sqrt{\frac{\epsilon_y}{\beta_y^*(0)}} = \phi_y^* \quad (ZZ)$$

Substituting Eq.(20) into (ZZ) it is readily concluded that

$$\theta_x^* = \phi_y^* = \left(\frac{\alpha_D}{M_x}\right)^{\frac{1}{2}} \cdot \left[\frac{\epsilon_x}{2 R_{11}(0) U_{1266}}\right]^{\frac{1}{4}} \quad (AA)$$

It is also interesting to note that

$$\sigma_x^*(0) \cdot \sigma_y^*(0) \simeq \frac{M_y \epsilon_y}{\alpha_D} \cdot [2 \epsilon_x R_{11}(0) U_{1266}]^{\frac{1}{2}} \quad (24)$$

The *total spot size* in each plane may then be calculated by folding the first- and higher-order effects together. The smallest total spot size that is achievable may be found by varying the first-order $\beta_x^*(0)$ and $\beta_y^*(0)$ around the above values until a minimum total spot size is found. This exercise is easily done using a ray tracing program such as TURTLE⁶. Obviously the minimum *total spot size* will be somewhat greater than the first-order size calculated by the above equations. Typical examples for the SLC are shown below in Figs. 8 through 11.

Within the space limitations of the SLAC site and with conventional room temperature quadrupole triplets, the design values applicable to the MarkII detector, for the parameters appearing in the above equations are the following:

$$l^* = 2.82 \text{ meters}, \quad M_x = M_y = 1/4, \quad \alpha_D = 1/57.$$

For the North final focus system (Electrons)

$$[R_{11}(0) U_{1266}] \simeq 354 \text{ meters} \quad [R_{33}(0) U_{3466}] \simeq 159 \text{ meters}$$

and for the South final focus system (Positrons)

$$[R_{11}(0) U_{1266}] \simeq 429 \text{ meters} \quad [R_{33}(0) U_{3466}] \simeq 169 \text{ meters}$$

as calculated from third-order TRANSPORT.

For the SLD detector superconducting quadrupoles will be used and the parameters change to the following for the TRANSPORT file called SUP1D FFS:

$$l^* = 2.21 \text{ meters}, \quad M_x = M_y = 1/5, \quad \alpha_D = 1/57, \text{ and}$$

$$[R_{11}(0) U_{1266}] \simeq 236 \text{ meters} \quad [R_{33}(0) U_{3466}] \simeq 167 \text{ meters}$$

4. Emittance Growth in the Chromatic Correction Section Dipoles

As stated above there is a practical limit to the maximum size of the dipole bending angle α_D . This is imposed by the emittance growth that results from the quantum fluctuations in the synchrotron radiation energy losses as the beam traverses the CCS dipoles. The emittance growth is a very sensitive function of the beam energy and of α_D . For each dipole it can be expressed in the following form:

$$\Delta\epsilon = K \cdot 10^{-11} \left[\frac{E \alpha_D}{2} \right]^5 \cdot \frac{1}{L_D} \text{ meters} \quad (25)$$

where K is a numerical factor that depends upon the beam parameters at the dipole⁴, E is the beam energy in GeV and L_D is the length of the dipole in

meters. K typically falls in the range of 4 to 12 depending upon the magnitude of the dispersion function within the dipole. However the more important point is that the emittance growth varies as the fifth power of the bending angle α_D .

So it is necessary to limit the size of α_D in order to keep $\Delta\epsilon$ sufficiently small. Because of the large exponent in Eq. 24 this will typically occur somewhere in the range of

$$\frac{1}{2E} \leq \alpha_D \leq \frac{1}{E} \quad (26)$$

For the SLC design, where $p_0 = 50 \text{ GeV}$, the bending angle α_D of each dipole in the CCS was chosen to be approximately $1/E$, *i.e.* one degree. This was large enough to significantly reduce, but not eliminate, the geometric aberrations listed above.

5. Emittance Growth in the Interaction Region Quadrupoles

K. Oide⁵ has shown that the quantum fluctuations occurring in the last quadrupole of a final focus system represents another limit on the minimum size of the beam that can be attained at the interaction point. This is a function of the normalized emittance, ϵ_N , of the beam and may be expressed as follows:

$$\sigma^* \simeq 3.5 \times 10^{-4} (\epsilon_N)^{\frac{5}{7}} \text{ meters} \quad (27)$$

where $\epsilon_N = \gamma\epsilon$.

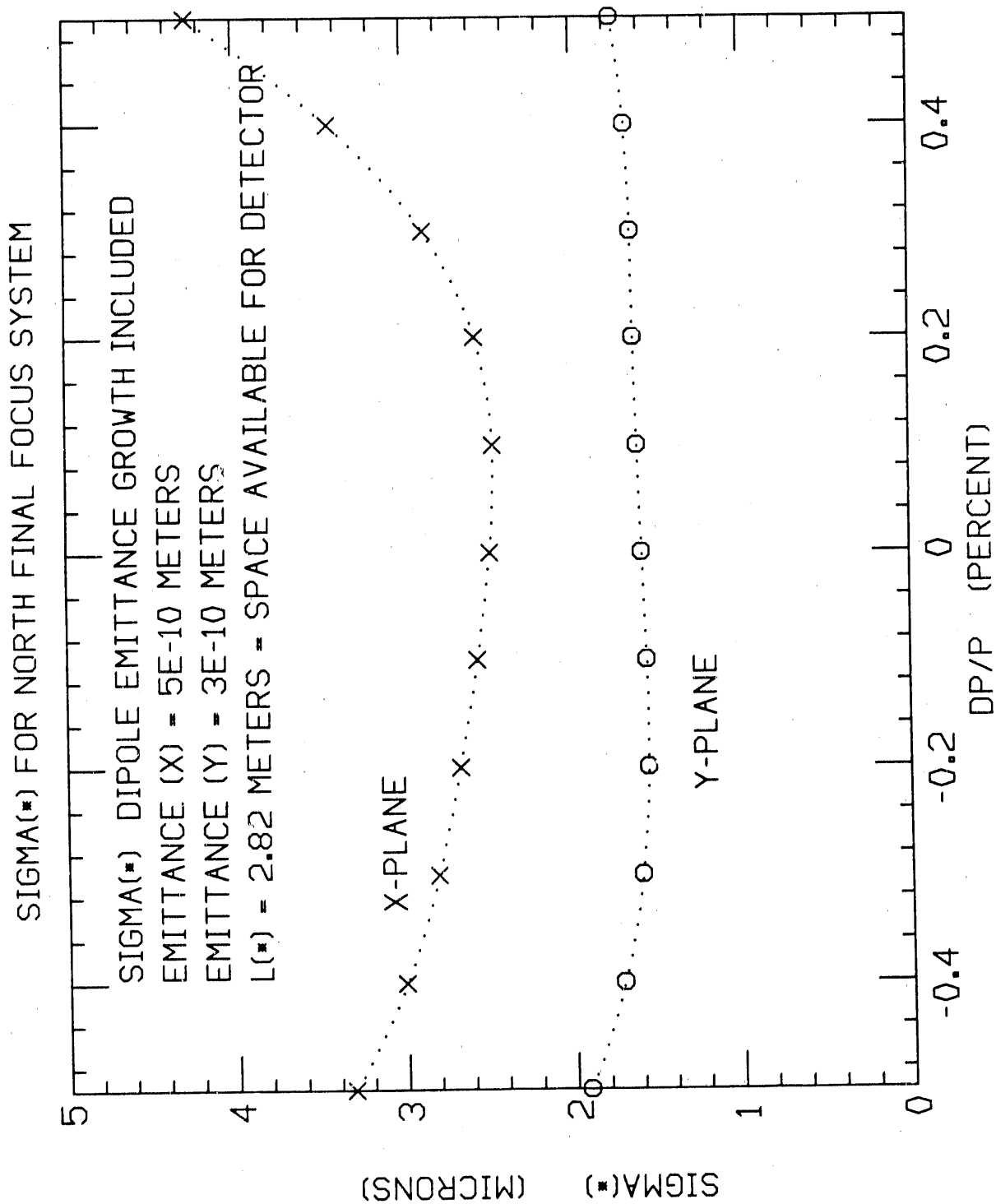
This result is of greatest interest at high energies and for flat beam final focus systems, where the beam size in the y plane is much smaller than in the x plane. For the SLC system it is *not a problem* because the limiting beam size calculated from Eq. 19 is 0.2 microns, which is significantly smaller than the theoretical round beam design size of 1 to 2 microns.

6. Examples

In Figs. 8 through 11 we show the result of computer simulations, using TURTLE⁶, for the values of $\sigma_x^*(\delta)$ and $\sigma_y^*(\delta)$, as a function of momentum, at the

interaction point. The plots using the symbols X for the x plane and O for the y plane show the effects of the higher-order geometric and chromatic aberrations. These results are representative of what is to be expected with real beams in the control room. The single points, represented by the asterisk symbol at $\delta = 0$ are the calculated values of $\sigma_x^*(0) = \sqrt{\beta_x^*(0) \epsilon_x}$ and $\sigma_y^*(0) = \sqrt{\beta_y^*(0) \epsilon_y}$ using Eqs. 20 and 22.

In Fig. 8, we show the predicted beam size, as a function of momentum for the Mark II detector for a beam emittance $\epsilon_x = \epsilon_y = 3 \cdot 10^{-10}$ meters. Fig. 9 shows the expected results when $\epsilon_x = 9 \cdot 10^{-10}$ meters and $\epsilon_y = 5 \cdot 10^{-10}$ meters. Fig. 10 shows the predicted beam sizes for the SLD detector for the design emittance in the x and y planes of $3 \cdot 10^{-10}$ meters. Fig. 11 is the result when $\epsilon_x = 9 \cdot 10^{-10}$ meters and $\epsilon_y = 5 \cdot 10^{-10}$ meters.



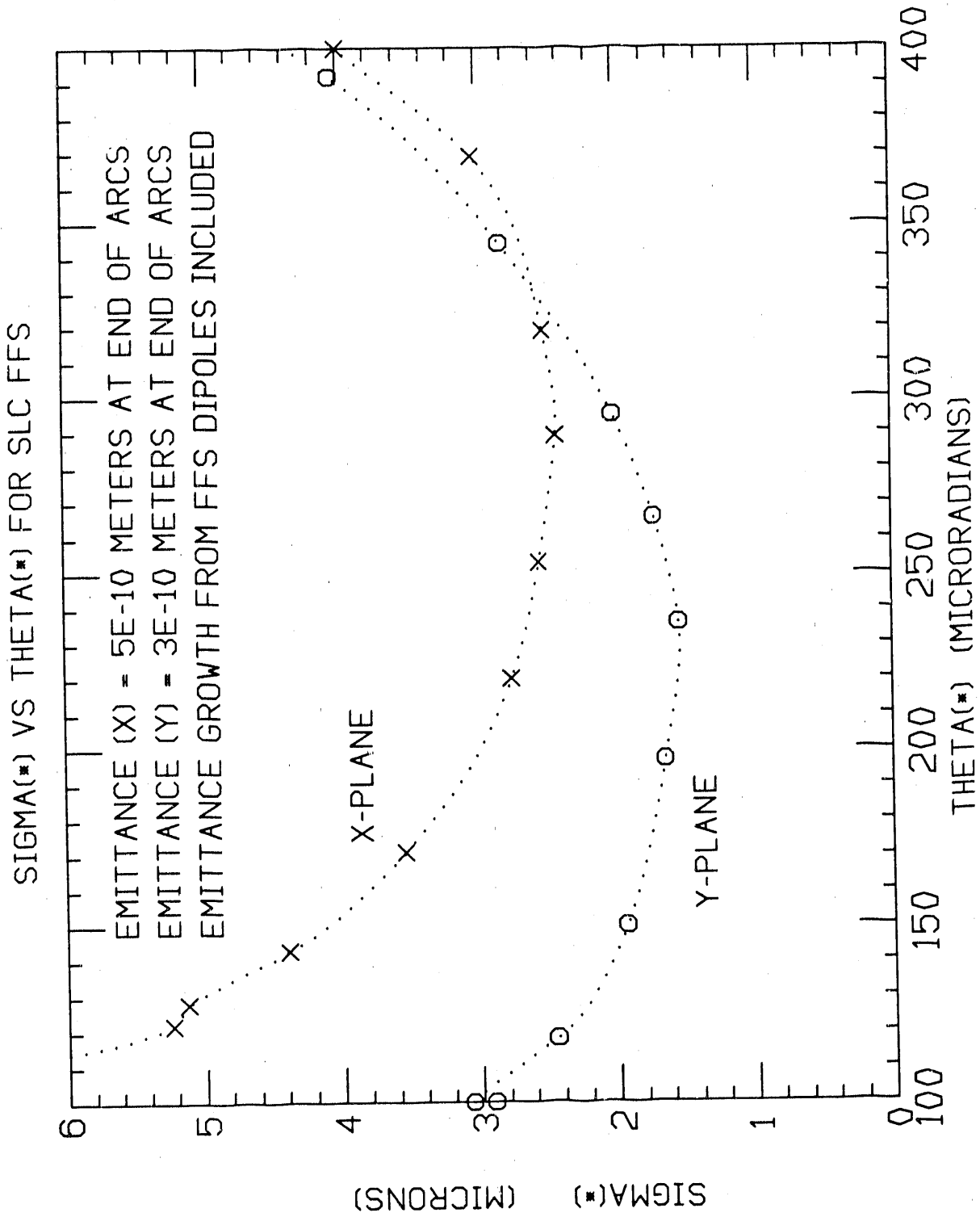


FIG. 8 SIGMA(σ) FOR THE AS BUILT SLC FINAL FOCUS SYSTEM

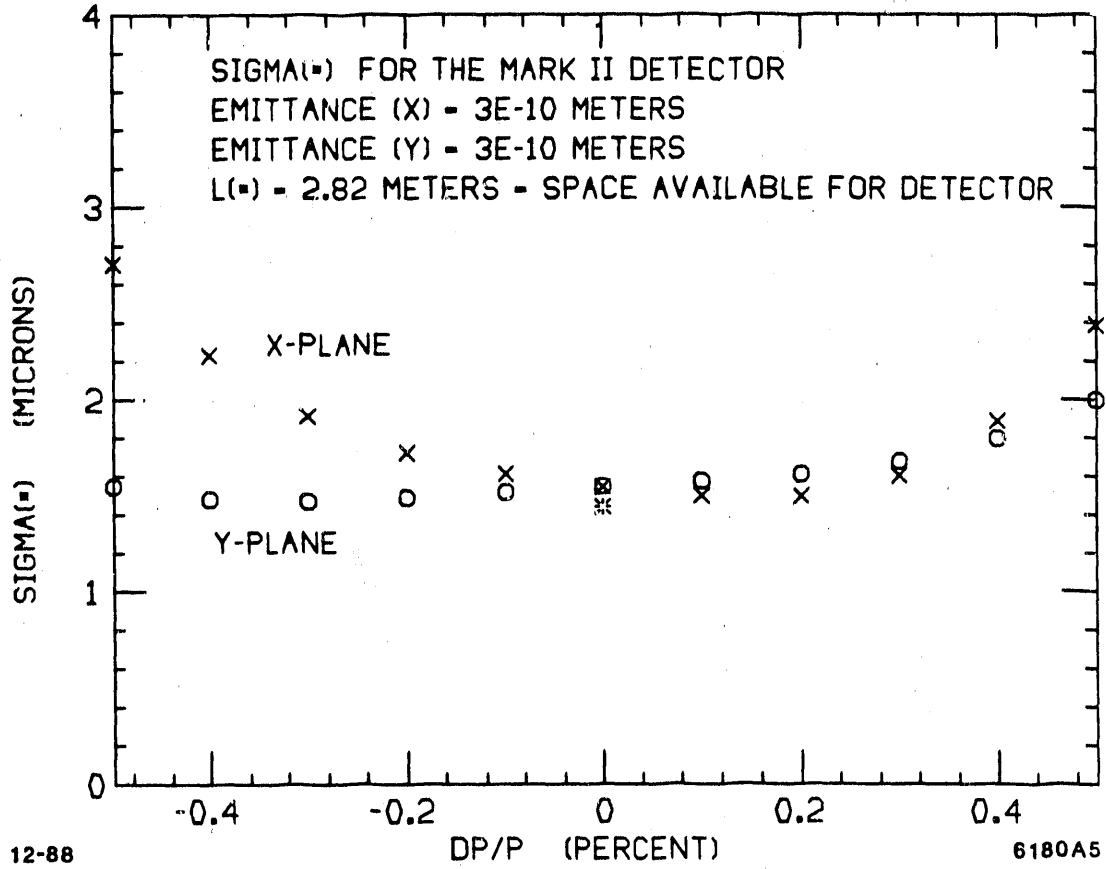


FIG. 8B SIGMA(▪) FOR THE AS BUILT SLC FINAL FOCUS SYSTEM

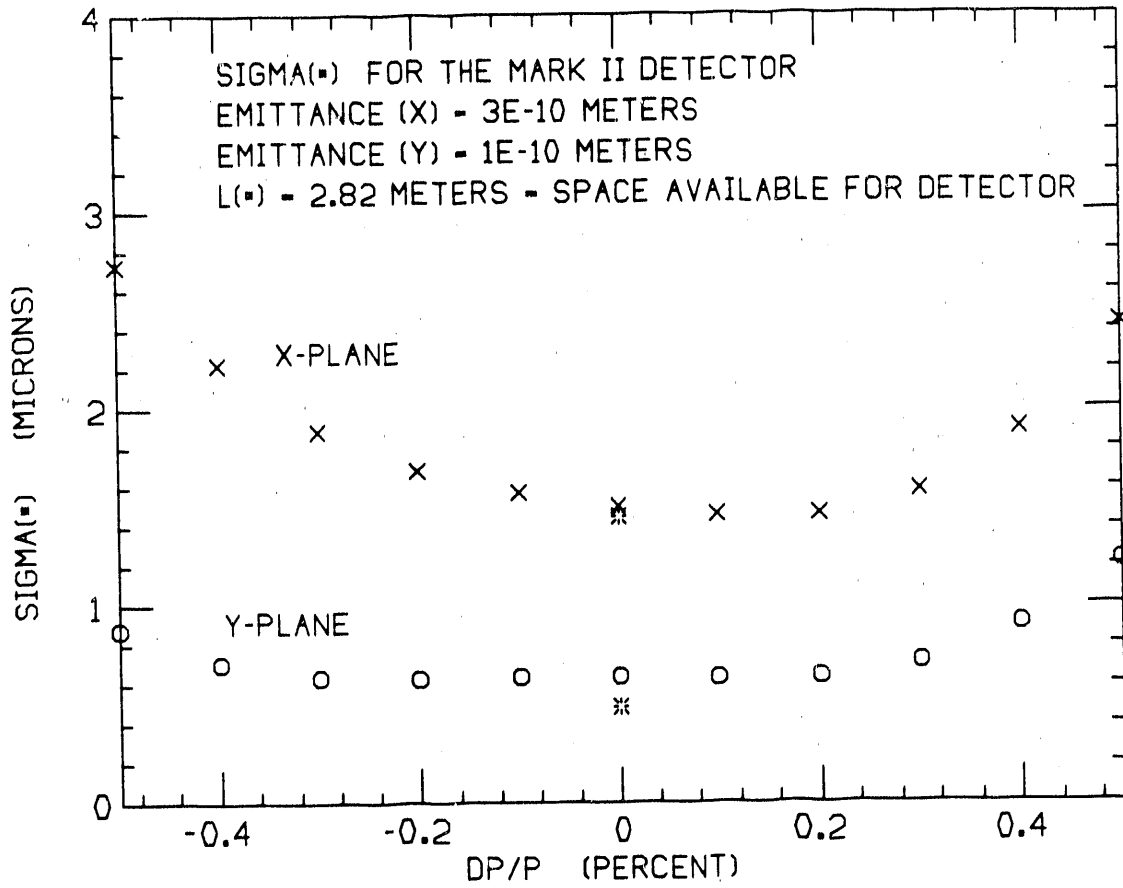


FIG. 9 SIGMA(σ) FOR AS BUILT SLC FINAL FOCUS SYSTEM

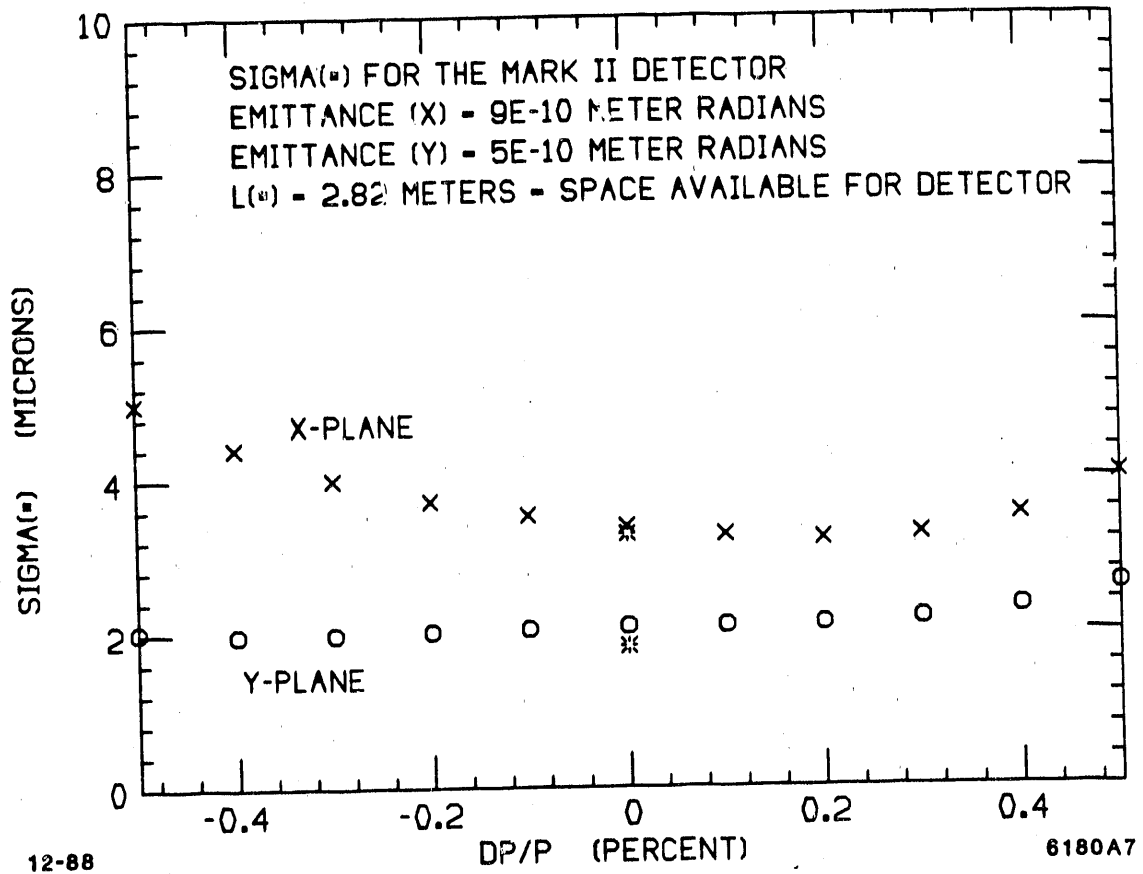


FIG. 10 SIGMA(σ) FOR AS BUILT SLC FINAL FOCUS SYSTEM

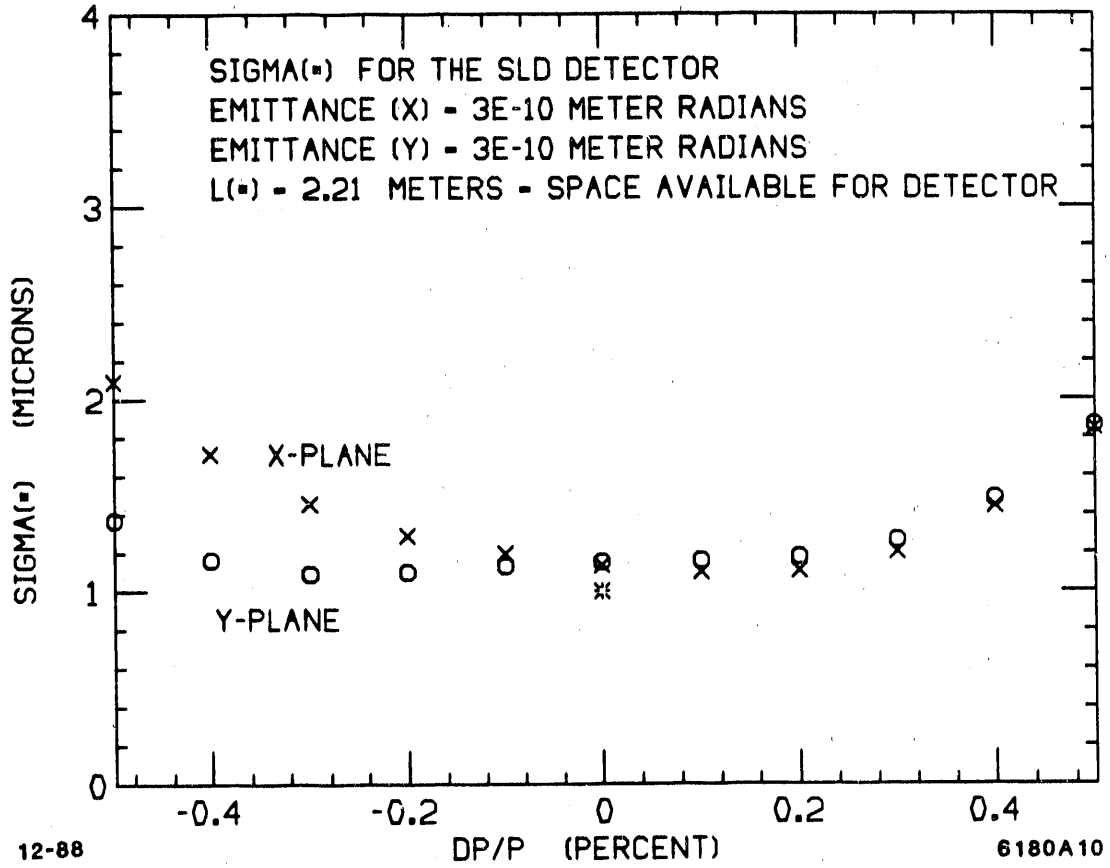
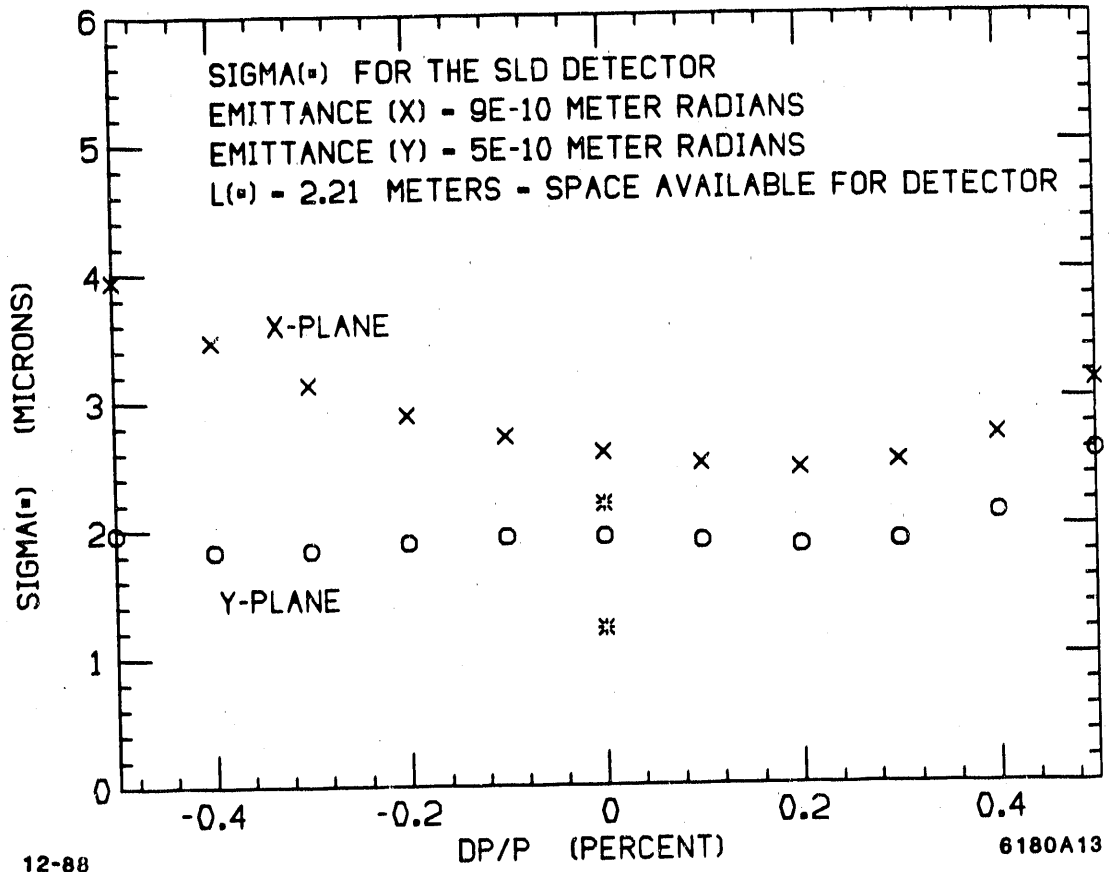


FIG. 11 SIGMA(σ) FOR AS BUILT SLC FINAL FOCUS SYSTEM



APPENDIX

7. Scaling Laws for Triplets and Doublets in the Interaction Region

In the SLC design the last lens module nearest the interaction point is a symmetric quadrupole triplet³. The reason for this is that the system is designed to produce round beam spots at the I.P. If a flat beam spot is desired then a quadrupole doublet is more appropriate. It is useful to have a simple triplet or doublet module as a starting point for a design that is easily scaled to different l^* values or to different energies. Two such modules are illustrated in Figs. 12 and 13.

The symmetric triplet module illustrated in Fig. 12 has been optimized to provide the maximum l^* for a given total length L_T . It has also been designed to have the same chromatic distortion in the x and y planes in anticipation of a round beam spot. The optical fitting condition for the module is shown by the R matrix in Fig. 12 and corresponds to simultaneous point to parallel and parallel to point imaging, *i.e.* a 90 degree phase shift in both planes. If one desires to scale the system keeping the same optical constraints, then the kl of every element of the system should remain constant, where $k^2 = B_0/aB\rho$, l is the length of the element and B_0/a is the field gradient. We may therefore express a scaling law for the triplet in the following form:

$$L_T \left[\frac{B_0}{aB\rho} \right]^{\frac{1}{2}} \geq \frac{16}{3} \quad (28)$$

where L_T is the total length of the module and $l^* \simeq \frac{L_T}{4}$.

The numerical constant on the right side of the equation has been determined empirical by fitting the optical constraints using TRANSPORT¹. The inequality sign allows for the possibility that one may not choose to scale the separation distance, d , between quadrupoles but instead fix its value to the minimum distance that is acceptable for a good engineering design. Our model assumes that the field gradients in all of the quadrupole elements are the same but the lengths of the

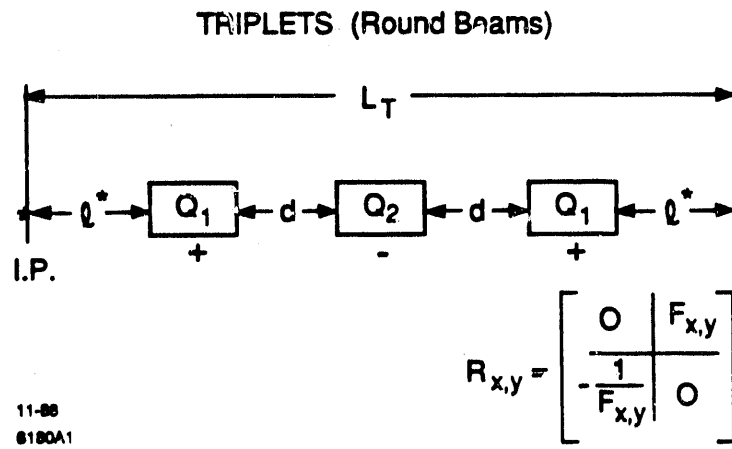


Fig. 12. A Symmetric Quadrupole Triplet Module.

elements are allowed to vary during the fitting process.

A similar scaling law for the doublet has the form:

$$L_D \left[\frac{B_0}{a B \rho} \right]^{\frac{1}{2}} \geq \frac{10}{3} \quad (29)$$

where L_D is the total length of the doublet module, and $l^* \simeq \frac{L_D}{3}$.

This module is shown in Fig. 13 along with the optical constraint used to fit it. It differs from the triplet in that only point to parallel imaging is imposed in each plane since lack of left right symmetry does not allow the possibility of simultaneous point to parallel and parallel to point imaging in the doublet.

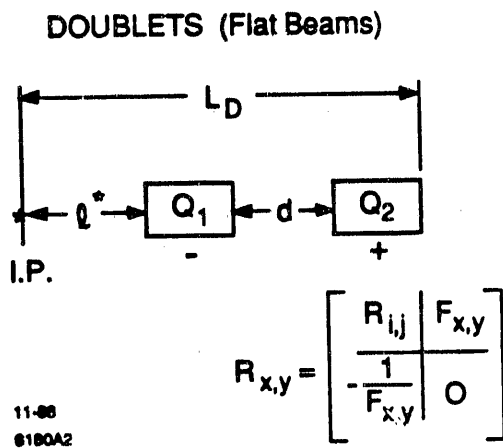


Fig. 13. A Quadrupole Doublet Module.

REFERENCES

1. K.L. Brown, D.C. Carey, C. Iselin, and F. Rothacker, TRANSPORT, A Computer Program for Designing Charged Particle Beam Transport Systems, SLAC-91 (1973 rev.), NAL-91, and CERN 80-04.
2. K.L. Brown and R.V. Servranckx, First- and Second-Order Charged Particle Optics, SLAC-PUB-3381, July 1984.
3. Karl L. Brown, A Conceptual Design of Final Focus Systems for Linear Colliders, SLAC-PUB-4159, June 1987, and J.J. Murray, K.L. Brown and T. Fieguth, The Completed Design of the SLC Final Focus System, SLAC-PUB-4219, February 1987.
4. H. DeStaebler, private communication, May 1981, and Matthew Sands, Emittance Growth from Radiation Fluctuations, SLAC/AP-47, December 1985.
5. Katsunobu Oide, A Final Focus System for Flat-Beam Linear Colliders, SLAC-PUB-4660, June 1988.
6. D.C. Carey, K.L. Brown, and Ch. Iselin, TURTLE, A Computer Program for Simulating Charged Particle Beam Transport Systems, Including Decay Calculations, SLAC-Report-246, March 1982.

END

DATE FILMED

02 / 20 / 91

